Journal of Applied Polymer Science

Inverted organic solar cells using nanocellulose as substrate

Saionara Vilhegas Costa,[1] Patrick Pingel,[2] Silvia Janietz,[2] Ana Flávia Nogueira[1]
[1]University of Campinas, Laboratório De Nanotecnologia E Energia Solar, Campinas-SP, PO Box 6154, 13083970, Brazil
[2]Fraunhofer IAP, Department Polymer and Electronics, Geiselbergstraße 69, Potsdam-Golm 14469, Germany
Correspondence to: A. Flávia Nogueira (E-mail: anaflavia@iqm.unicamp.br)

ABSTRACT: Organic photovoltaics (OPVs) offer the potential for ultralow cost mass-producible photovoltaic devices. Other advantages are light weight and good mechanical flexibility. To further reduce the cost, the replacement of the conventional conducting substrates for cellulose is an interesting choice. There are three main types of nanocellulose materials: nanofibrillated cellulose (NFC), nanocrystalline cellulose (CNC), and bacterial nanocellulose. In this work, the synthesis of two types of nanocellulose substrates and their application in OPVs were achieved. For the first time, the different properties of the cellulose substrates and their influence on the OPV performance were addressed. The nanocellulose substrates CNC and NFC were characterized by XRD, AFM, and DSC. CNC films were more homogeneous, smoother, crystalline and with low roughness. Thus, when comparing the cellulosic substrates, the best device the one based on CNC. The PCE values of the inverted OPV cells were 3.0, 1.4, and 0.5% on to glass, CNC and NFC substrates. © 2016 Wiley Periodicals, Inc. J. Appl. Polym. Sci. **2016**, *133*, 43679.

KEYWORDS: biopolymers and renewable polymers; cellulose and other wood products; optical and photovoltaic applications

Received 10 December 2015; accepted 23 March 2016
DOI: 10.1002/app.43679

INTRODUCTION

Organic photovoltaics (OPVs) have emerged as potential economical alternative to silicon-based solar cells due to their low-cost fabrication by solution processing, lightweight and compatibility with flexible substrates.[1] Over the last decade, the power conversion efficiency (PCE) of small-area organic solar cells has improved and achieved values higher than 10%.[2–4] OPVs are usually assembled in two configurations, conventional and inverted.[5] The inverted configuration offers the advantage of long-term stability, because the electrode compositions are robust to both oxygen and humidity.[6] Many studies have been done in the development of new materials, device geometries and interfaces in an attempt to improve OPV performance.[6] In general, flexible OPVs use polyethylene terephthalate (PET),[7] polyethylene naphthalate (PEN),[8] or polyethersulfone (PES)[9] as substrates. However, their high cost (as they use ITO as conducting layer) and their plastic nature, inspire the researchers to search for new cost-effective and easily recyclable or biodegradable substrates. Recent reports demonstrate that transparent cellulose based on nanofibers substrates may replace the plastic ones because of their advantages like biodegradability, abundant in nature, lower cost, minimal use of toxic chemicals, and recyclability.[10]

Cellulose is one of the most ubiquitous and abundant natural polymers on the planet. Cellulose fibers have diameter of 20–50 μm and are made up of thousands of microfibrils with diameters of a few to tens of nanometers. Cellulose fibers can form a smoother, less scattering film than a common paper.[11] Depending on the preparation method, there are three main types of nanocellulose: nanofibrilated cellulose (NFC), nanocrystalline cellulose (CNC) and bacterial nanocellulose.[12] NFC, CNC, and bacterial nanocellulose are prepared by the delamination of the wood pulp using mechanical pressure, chemical, or enzymatic treatment, acid hydrolysis of cellulose and bacterial synthesis, respectively.[12] CNC and NFC have unique properties including high E (Young's modulus—describes tensile elasticity), dimensional stability, low thermal expansion coefficient, outstanding reinforcing potential, and transparency.[13]

Cellulose fibers can be used to make transparent films,[13] such property is suitable to produce highly transparent and smooth substrates.[11,14] These properties make these films an interesting alternative for substrates in the electronic industry. A wide variety of devices have been made using the aforementioned transparent paper substrates, including organic light-emitting diodes (OLED),[15] organic solar cells,[10,13] touch screens, thin film transistor,[14] biological, and chemical sensors.[16]

Few reports in the literature investigate the use of nanocrystalline cellulose as substrate in organic solar cells.[10,13] In both cases, the authors used the nanocrystalline cellulose as substrate

Additional Supporting Information may be found in the online version of this article.

but the correlation with the device efficiency and cellulose properties was not evaluated.

First, we studied how the preparation conditions may lead to an ideal smoothing cellulose film. Thus, polymer concentration, use of a plasticizer, choice of the method to homogenize the cellulose solution and others parameters were addressed and the resulting films were tested as substrates in organic solar cells. Two different types of cellulose, nanocrystalline, and nanofibrillated were employed in this work. The goal of this work is to find out which type of cellulose would form more suitable films for subsequent use in inverted organic solar cells and yet, which the main properties of cellulose films are more important for further improvement. We concluded that the most important properties are related to the surface roughness, crystallinity, scattering of the fibers, and uniformity of the film.

EXPERIMENTAL

Materials

1,2 dichlorobenzene 99%, 2-methoxyethanol $\geq$ 99.9%, glycerol $\geq$ 99% were purchased from Sigma-Aldrich (Germany), polyethylenimine (PEI) 50% w/v in H_2O, Fluka, ZnO:Al solution was provided by Nanograde N-10X®, nanoparticle size ca. 15 nm, 98 wt % ZnO, 2 wt % Al_2O_3).

The active layer was composed by the amorphous polymer poly{9,9-dioctylfluorenyl-2,7-dyil-co-[10,12-*bis*(thiophen-2-y)-3,6-dioxooctyl-11-thia-9,13-diaza-cyclopenta[b]triphenylene}-(PFDTBTP) combined with $PC_{70}BM$ (Phenyl-C71-butyric-acid-methyl ester, 99%, purchased from Solenne). PFDTBTP was synthesized in our laboratory via a Suzuki C—C-crosscoupling reaction.[17]

Ag, 99.99%, granulate 0.7–1.5 mm, purchased from Umicore, MoO_3, 99.95%, sublimed powder, purchased from Alfa Aesar.

Two types of cellulose were tested: nanocrystalline cellulose (CNC) powder from the University of Maine (EUA) and nanofibrillated cellulose (NFC) solution from Fraunhofer IAP, Department Biopolymers (Germany). Cellulose nanocrystals are rod-like particles with dimensions of approximately 5 nm diameters and 150–200 nm length, this cellulose was manufactured from wood pulp as the raw material. NFC has diameter around of ~4 nm and length of hundreds of nanometers.[18] The degree of polymerization of CNC and NFC are 186 and 250–600, respectively.

Methods

Preparation of Cellulose Films. The cellulose films were prepared by stirring in a magnetic stirrer (IKA® RCT basic IKAMAG™ safety control, universal hot plate magnetic stirrer, 1500 rpm, 230 V) and also using an ultrasonic homogenizer (Sonoplus HD 2200, Bandelin electronic GmbH & Co.) for 5 min (100% Power, Cycle 90%) (Supporting Information Figure S1).

Nanocrystalline Cellulose (CNC). In order to obtain a homogeneous film, nanocellulose aqueous solutions were tested with and without glycerol as plasticizer. In fact, homogeneous films, without the presence of bubbles were obtained only after addition of glycerol. The experiments were performed according to Supporting Information Table SI. The aqueous solutions of cellulose and glycerol were prepared separately and stirred for a few minutes. After 30 min of magnetic stirring, the solutions were placed in the same container under magnetic stirring for 12 h or ultrasonic homogenizer (Supporting Information Figure S1). Then the solutions (45 mL) were deposited on a plastic Petri dish and placed in an oven at 45 °C for 2 days.

Nanofibrillated Cellulose (NFC). Aqueous solutions of nanofibrillated cellulose were prepared with 1 wt % of NFC (no glycerol was added). The solutions were left under magnetic stirring and heated to 50 °C during 30 min to homogenize the solution. After this, a volume of 45 mL was transferred to a plastic Petri dish and allowed to evaporate for 2 days at 45 °C.

Characterization of the Nanocellulose Films. Nanosurf AFM was used to image the surface topography in the noncontact/phase contrast mode. A surface profiler (Dektak 150) was used to measure the layer thickness. The scanning electron microscope (SEM) images were obtained through a JEOL JSM-6360LV with acceleration of 5 kV.

The nanocellulose films were characterized by X-ray diffraction technique using a Shimadzu-XDR 7000 diffractometer equipped with a copper tube and a graphite monochromator and operated at a power of 40 kV and 35 mA.

Differential scanning calorimetry (DSC) analysis (3–5 mg per cellulose sample) was carried out in a Netzsch DSC 204 Phoenix with a scanning rate of 10 K/min. The glass transition temperature was obtained from the second heating cycle. The DSC curves were measured from −70 to 300 °C (Supporting Information Figure S8). The thermogravimetry (TGA) analysis of the cellulose films was obtained in a TGA 2950 Thermogravimetric Analyzer of TA Instruments apparatus. The curve was conducted under constant flow of argon (100 mL/min). Samples were heated from room temperature to 1000 °C with a heating rate of 10 °C/min (Supporting Information Figure S9). UV/Vis analysis was obtained in a Cary 5000 UV/Vis spectrometer.

Solar Cell Assembly. Inverted organic solar cells were fabricated using two different substrates: cellulose films and transparent glass (e.g., nonconducting glass). However, due to the fragile nature of the cellulose films, they were glued onto a glass substrate by a doubled sided tape. In both cases, the configuration is: substrate/Ag/ZnO:Al/PFDTBTP:$PC_{70}BM$/MoO_3/Ag with an active area of 0.09 cm^2 (see—Graphical Abstract). The energy levels are presented in Figure 1(a). The chemical structures of the polymer PFDTBTP and $PC_{70}BM$ are also shown in Figures 1b, c, respectively.

Silver (20 and 100 nm) and MoO_3 (8 nm) were thermally evaporated. ZnO:Al films were deposited by spin-coating inside a glove box. The solution was deposited at 1200 rpm for 30 s, and heat treated 120 °C during 20 min.

PFDTBTP:$PC_{70}BM$—PFDTBTP was combined with $PC_{70}BM$ in a weight-to-weight ratio of 1:2, active layers were deposited from 15 and 45 mg/mL solutions in 1,2 dichlorobenzene on the top of the substrate/Ag/ZnO:Al, where the substrates are glass or cellulose films.

The thickness the active layer was 60 nm on glass and 300 nm on cellulose. In order to further improve the efficiency of the solar cells and lower the leakage current, a thin layer of

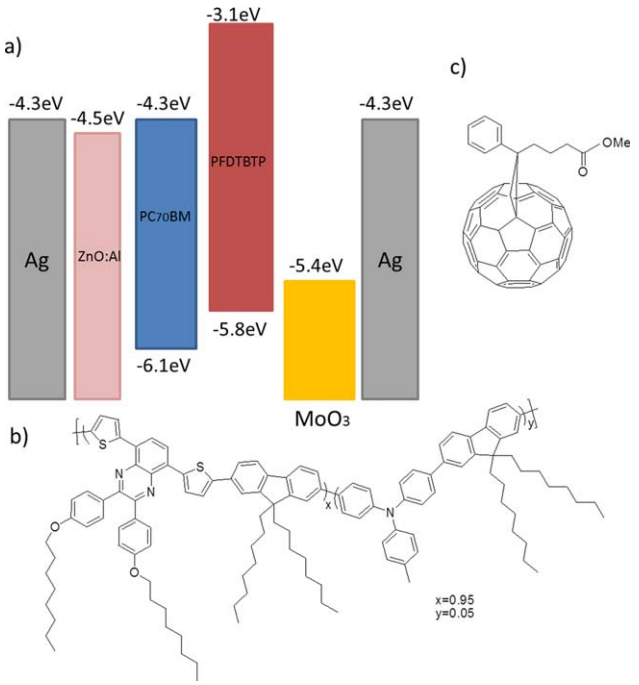

Figure 1. (a) Energy level diagram. (b) Chemical structure of PFDTBTP. (c) Chemical structure of $PC_{70}BM$. [Color figure can be viewed in the online issue, which is available at wileyonlinelibrary.com.]

polyethylenimine (PEI) was incorporated in the cells to act as an electron transport layer. The PEI solution was prepared at 0.1% wt (10 mg PEI solution 50% v/v was dissolved in 10 g of 2-methoxyethanol). The solution was deposited at 4500 rpm for 30 s and heat at 130 °C during 15 min. The thickness of the PEI layer was around 10 nm.

During the deposition process of the active layer PFDTBTP:$PC_{70}BM$, two parameters were varied. The speed tested was 500 and 600 rpm during 30 s and the solution evaporation was carried out at 70 °C during 20 min or let in the glove box at room temperature overnight.

A light source from K.H. Steuernagel was used to illuminate the solar cells (~100 mW/cm^2) while measuring the current density–voltage characteristics with a SMU from Keithley. A silicon reference diode with a KG3 filter, which was calibrated at Fraunhofer ISE, was used to adjust the intensity of the light source before measuring the devices.

The series resistance was calculated by $R_s = (di/dv)$ at zero potential ($V = 0$), and shunt resistance was obtained $R_{sh} = (di/dv)$ at current zero ($I = 0$).

RESULTS AND DISCUSSION

Nanocellulose Films

To evaluate how the solution and the film transparency are affected by the preparation conditions, we employed two different equipments to prepare the cellulose solution: a common magnetic stirrer and an ultrasonic homogenizer. The ultrasonic homogenizer gave rise to a solution with higher transmittance (Figure 2) and consequently, a transparent film, thus this procedure was adopted.

It was noted that the nanocellulose film prepared with an ultrasonic homogenizer showed higher transparency (Figure 2). Both CNC and NFC presented good flexibility and mechanical

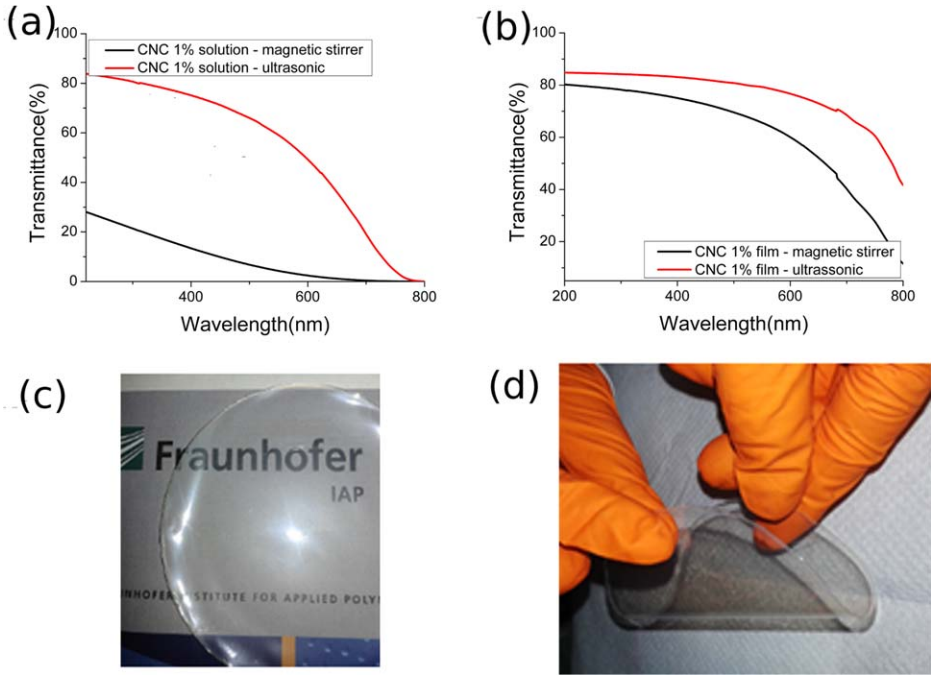

Figure 2. Transmittance of the cellulose solution and films obtained by magnetic stirring during 12 h (Black) and ultrasonic homogenizer for 5 min (Red). (a) Cellulose solution. (b) Cellulose films. (c) and (d) Images of the nanocellulose CNC films after the evaporation process. [Color figure can be viewed in the online issue, which is available at wileyonlinelibrary.com.]

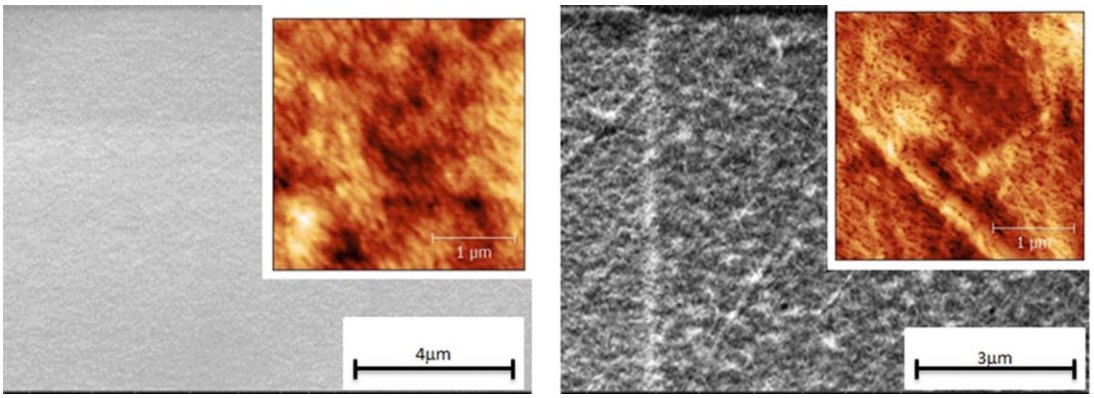

Figure 3. SEM images of (a) nanocrystalline cellulose (CNC) film from 1 wt % aqueous solution containing glycerol as plasticizer, (b) nanofibrillated cellulose (NFC) film from 1 wt % aqueous solution: Inset AFM images: topography forward. Area 3 × 3 μm. [Color figure can be viewed in the online issue, which is available at wileyonlinelibrary.com.]

properties. Films prepared only with magnetic stirring are more heterogeneous, and bubbles can be visualized inside the film (Supporting Information Figure S2).

The films obtained from crystalline nanocellulose were prepared with different concentration of CNC (1, 1.2, and 1.65 wt %) and 1 wt % of glycerol in aqueous solution. Whereas, nanofibrillated cellulose films were prepared with 1 wt % NFC without glycerol. Addition of glycerol in NFC originated films with many bubbles and high degree of heterogeneity. The films obtained from nanocrystalline cellulose/nanofibrillated cellulose materials showed thickness values of 45–50 μm/35 μm, respectively. The difference in transmittance of the nanocrystalline and the nanofibrillated cellulose films is depicted in Supporting Information Figure S3. The limited transmittance of the cellulosic films is believed to be due to scattering, not absorption, caused by the random distribution of the nanocrystals and nanofibers in the films.[13] Before employing the substrates in organic solar cells, the films were submitted to tests of variation of the mass along temperature. In this preliminary test, it was possible to compare samples with different mass of the nanocellulose substrate at the temperature of 45, 100, and 130 °C. It was found that in the film treated at 45 °C, only a small change of the total mass from 1.51 to 1.46% has occurred, it means that only a small portion of water was removed after 45 °C resulting in 0.05% loss of total mass (Supporting Information Figure S4). The XRD showed that there is a difference in the crystallinity in the different cellulosic films, CNC, and NFC. Both the films presented characteristic peaks of cellulose with similar intensities. The intensity of the signal from the (110) and (200) planes of the CNC is more intense, indicating a more crystallinity order (Supporting Information Figure S5). The peak related to the (110) plane in the NFC film is wider, confirming a more amorphous character of the NFC film. SEM images (Figure 3) showed that CNC film has homogeneous surface with well distribution of crystals throughout the film, whereas NFC film has a more fibrous heterogeneous surface with easily detached fibers. To gain information about morphology, we imaged the cellulose films surfaces by AFM, and the topography images are shown inset in Figure 3. In the AFM images (topography forward in the area 10 × 10 μm), it was possible to analyze the roughness, uniformity of the scattering centers, and shape fibers.

The topography images reveal that in the case of the nanofibrillated cellulose films, the fibers are more heterogeneously spread over the film and concentrated in some regions. This feature provides nanofibrillated cellulose films with higher roughness values when compared to the nanocrystalline cellulose film (Table I). The roughness values for CNC and NFC (area 3 × 3 μm) were $R_{ms} = 7.9$ and $R_{ms} = 20.2$ nm, respectively. For a larger area (10 × 10 μm), the roughness values were $R_{ms} = 8.3$ and $R_{ms} = 10.9$ nm, respectively. We believe that the higher difference in R_{ms} values between the CNC and NFC in the small area 3 × 3 μm is because of the image acquisition was obtained in the fiber surface.

To understand the thermal stability of the nanocellulose substrates, DSC and TG/DTA experiments were performed and the results are depicted in Supporting Information Figures S6 and S7, respectively. All cellulose films (CNC and NFC) have the same behavior through DSC and TG/DTA analysis. In the DSC, the first peak (74.1 °C) indicated the final water evaporation and

Table I. Cellulose Films Roughness Values

Roughness values			
Nanocrystaline cellulose (CNC)		Nanofibrillated cellulose (NFC)	
Area 3 × 3 μm	Area 10 × 10 μm	Area 3 × 3 μm	Area 10 × 10 μm
R_{ms} = 7.9 nm	R_{ms} = 8.3 nm	**R_{ms} = 20.2 nm**	R_{ms} = 10.9 nm
R_a = 6.3 nm	R_a=6.6 nm	R_a = 11.5 nm	R_a = 8.4 nm

[a] The standard deviation between the R_{ms} and R_a values were very low, error values around of 0.3 nm.

the second peak (237 °C) corresponds to cellulose decomposition. These results infer that it is possible to perform thermal treatments during OPV assembly up to 200 °C without damaging the cellulose substrates. The TG/DTA analysis corroborates with the DSC and polymer degradation occurs only after 217 °C.

Inverted Solar Cells Using Active Layer PFDTBTP:$PC_{70}BM$

The PFDTBTP donor polymer (see Figure 1) exhibits good absorption in the visible region (Supporting Information Figure S8) with two peaks at 391 and 530 nm.[17] The chemical synthesis of PFDTBTP has been described elsewhere.[17] The electrical parameters obtained from the IV curves (Figure 4) at 100 mW/cm^2 are presented in the Table II. The inverted solar cells on glass substrate presented $J_{sc} = 7.9$ mA/cm^2, $V_{oc} = 0.7$ V, FF = 0.5 and a PCE of 3.0%. The OPV assembled with CNC substrate delivered $J_{SC} = 3.5$ mA/cm^2, $V_{OC} = 0.9$ V, FF = 0.4 and a PCE of 1.4% and the OPV on NFC substrate $J_{SC} = 2.0$ mA/cm^2, $V_{OC} = 0.7$ V, FF = 0.3 and a PCE of 0.5%.

The donor polymer PFDTBTP was used in an organic solar cell in the normal configuration (ITO/PEDOT:PSS/PFDTBTP:$PC_{61}BM$/LiF/Al) using conventional TCO substrates (ITO). The active layer PFDTBTP:$PC_{61}BM$ was inkjet printed or spin coated and were obtained PCE of 3.7% with the solvents chloro-/trichlorobenzene and 2.7% with chlorine-free solvents.[19]

The OPV fabricated on cellulose substrates (Table II) presented lower fill factor because of the high values of both shunt and series resistance, as expected from less conducting substrates. CNC and NFC presented $R_S = 68$ and 206 Ω cm^2, $R_{Sh} = 602$ and 599 Ω cm^2, respectively. Although the shunt resistance values were very close in both cellulose substrates; the series resistance values were quite different. The high value of series resistance in the NFC devices is due to a more fibrous, heterogeneous and rough surface. This has a huge impact on the J_{SC} and FF values in the OPV assembled with NFC substrates compared to the solar cell on CNC substrate. The results are in agreement with the morphological characterization using AFM and FEG–SEM microscopies.

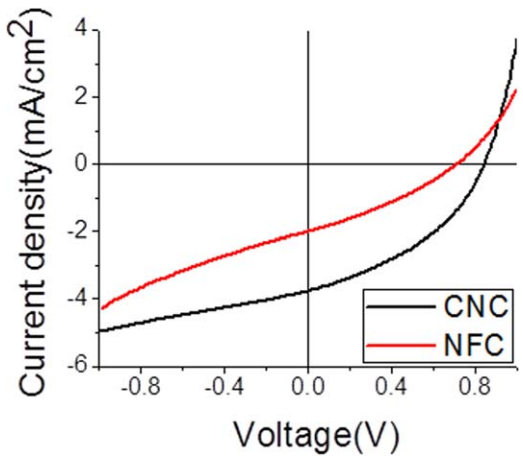

Figure 4. Current density versus voltage for solar cells with PFDTBTP:$PC_{70}BM$ on CNC (black) and on NFC (red). Under illumination at 100 mW/cm^2. [Color figure can be viewed in the online issue, which is available at wileyonlinelibrary.com.]

Table II. I–V Parameters of Inverted Solar Cells Using PFDTBTP:$PC_{70}BM$, 4.5 wt % Polymer on to Glass, CNC, and NFC Substrates (Table Values were Obtained by Averaging of Six Cells Mounted to Each Type of Substrate[a]

	Solar cells parameters			
Substrate	J_{SC} (mA/cm^2)	V_{OC}	FF	PCE %
Glass	7.9 ± 0.13	0.7 ± 0.14	0.5 ± 0.01	3.0 ± 0.74
CNC	**3.5** ± 0.27	**0.9** ± 0.01	**0.4** ± 0.01	**1.4** ± 0.10
NFC	**2.0** ± 0.06	**0.7** ± 0.29	**0.3** ± 0.03	**0.5** ± 0.22

[a] Error values was calculated with $E = s/\sqrt{n}$, s standard deviation and n is the number of samples.

The performance of the inverted OPV assembled with cellulose substrates is shown to be limited by the transmittance of the thin Ag layer (Supporting Information Figure S9), the semi-transparent bottom electrode. Besides, the reproducibility of the anode Ag film is not easy to achieve. However the use of the silver film as top electrode has several advantages as reported in the literature, including the oxidation to silver oxide. After Ag oxidation, the electrode work function increases from 4.3 to 5.0 eV,[20] similar to the gold work function (5.0 eV). Thus, the presence of a silver oxide layer in the top electrode should enhance the charge collection.[20]

Although the PCE of the solar cells using only PEI layer was very close to the devices with both ZnO:Al and PEI layers, introducing both PEI and ZnO:Al layers, we ensured the reproducibility of the devices with most of the solar cells with similar Voc and FF values. A high Voc value of 0.8 V was achieved in all solar cells mounted with PEI and ZnO:Al. This can be explained by the roughness values of the films containing only the PEI film with the films ZnO:Al and PEI layers presented in Supporting Information Table SII. It is possible to note that the substrates with the ZnO:Al on to Ag layers present higher roughness when there is only a layer of silver Ag. The R_{ms} values of the Ag onto CNC film were: $R_{ms} = 28.6$ nm (3 × 3 μm) and $R_{ms} = 23.3$ nm (10 × 10 μm). Incorporating ZnO:Al layer on the top of the Ag/CNC, the values obtained were $R_{ms} = 29.9$ nm (3 × 3 μm), $R_{ms} = 53.3$ nm (10 × 10 μm). The difference in the R_{ms} with and without ZnO:Al layer is very pronounced in a larger area. This occurs because of the sum of the deformities. In contrast, after introduction of a PEI layer on to the ZnO:Al film, we observed a significant decrease in the roughness values.

The decrease in roughness values is accordance with the best results in solar cells using PEI deposited on the top of the ZnO:Al layer. The smoothing surface allows fewer short circuits and lower loss of charge during the operation of the devices.

The work function values of the layers were obtained by photoelectron spectroscopy (Supporting Information Figure S10). In the configuration only with ZnO:Al layer (ZnO:Al/Ag/cellulose CNC) the value obtained was 4.41 eV and with PEI layer (PEI/ZnO:Al/Ag/cellulose CNC), 4.28 eV. The difference was 0.13 eV. The shift in the work function can be ascribed to the decrease in the electrostatic potential at the surface of the ZnO layer

caused by the surface dipoles. Such dipoles induce a formation of an ionic double layer between the electron-accepting ZnO surface (oxygen parts) and the electron-donating PEI surface (nitrogen parts).[21] This ionic double layer facilitates the flow of electrons to the electrode, which may result in an improved solar cell performance. However, we believe that the major contribution relies on the surface characteristics of the CNC substrate.

In Supporting Information Figure S11, we can see the damage that occurs on to the surface of cellulose-based solar cells after the IV measurements. This damage is the cause of short circuits in some devices, or even the lack of response in others.

Based on the results obtained in this work, we point out the necessity of a further investigation to improve the fragility of the cellulosic substrates for the subsequent application in electronic devices. The use of a composite cellulosic or a treatment on film's surface are interesting alternatives to improve the mechanical resistance of the substrates. However, our preliminary investigation demonstrated that CNC substrate exhibited higher performance than NFC substrates when applied in OPV and that the results obtained in this work has strong correlation with film morphology.

CONCLUSIONS

The inverted solar cells assembled on nanocrystalline cellulose (CNC) showed better performance than the solar cells assembled on nanofibrillated cellulose (NFC) substrate. Our results indicate that the best performance in the OPV assembled with the CNC substrate is strongly correlating to the properties of the cellulose film. Among the mainly properties stand out: roughness, crystallinity and homogeneity of the fibers throughout the film. In this work, transparent cellulose films were obtained using an ultrasonic homogenizer. This methodology can be extended in order to obtain cellulosic films for others flexible electronic devices. One of the main drawback is the transmittance losses found when a silver layer was employed as one of the contacts. In future works, this layer must be replaced for other more transparent conductive layer.

However, the inverted organic solar cells were assembled on both types of cellulose substrates using PFDTBTP:$PC_{70}BM$ as the active layer. As expected, the best device was obtained using CNC as substrate. ZnO:Al and PEI layers were also introduced to decrease the leakage current. The power conversion efficiency values (PCE) of the inverted OPV cells were 3.0%, 1.4% and 0.5% onto glass, CNC and NFC substrates respectively.

ACKNOWLEDGMENTS

The authors thank, Mr. Björn Gruber (Fraunhofer-IAP) for the AFM images and researcher Dr. Kay Hettrich—Department of Biopolymer in Fraunhofer IAP for donation of nanofibers solution. A.F.N and S.V.C thank FAPESP, INEO and CNPq for the fellowship and financial support.

REFERENCES

1. Christoph Richter, D. L.; Gueymard, C. A. Solar Energy; Springer: New York, **2013**.
2. Service, R. F. *Science* **2011**, *332*, 293.
3. Brabec, C. J.; Gowrisanker, S.; Halls, J. J. M.; Laird, D.; Jia, S.; Williams, S. P. *Adv. Mater.* **2010**, *22*, 3839.
4. Zhang, J.; Zhang, Y.; Fang, J.; Lu, K.; Wang, Z.; Ma, W.; Wei, Z. *J. Am. Chem. Soc.* **2015**, *137*, 8176.
5. Scharber, M. C.; Sariciftci, N. S. *Prog. Polym. Sci.* **2013**, *38*, 1929.
6. Subbiah, J.; Purushothaman, B.; Chen, M.; Qin, T.; Gao, M.; Vak, D.; Scholes, F. H.; Chen, X.; Watkins, S. E.; Wilson, G. J.; Holmes, A. B.; Wong, W. W. H.; Jones, D. J. *Adv. Mater.* **2015**, *27*, 702.
7. Nickel, F.; Haas, T.; Wegner, E.; Bahro, D.; Salehin, S.; Kraft, O.; A. Gruber, P.; Colsmann, A. *Solar Energy Mater. Solar Cells* **2014**, *130*, 317.
8. Logeeswaran, V. J.; Kobayashi, N. P.; Islam, M. S.; Wu, W.; Chaturvedi, P.; Fang, N. X.; Wang, S. Y.; Williams, R. S. *Nano Lett.* **2009**, *9*, 178.
9. Zhou, Y.; Fuentes-Hernandez, C.; Shim, J.; Meyer, J.; Giordano, A. J.; Li, H.; Winget, P.; Papadopoulos, T.; Cheun, H.; Kim, J.; Fenoll, M.; Dindar, A.; Haske, W.; Najafabadi, E.; Khan, T. M.; Sojoudi, H.; Barlow, S.; Graham, S.; Brédas, J. L.; Marder, S. R.; Kahn, A.; ; Kippelen, B. *Science* **2012**, *336*, 327.
10. Zhou, Y.; Khan, T. M.; Liu, J. C.; Fuentes-Hernandez, C.; Shim, J. W.; Najafabadi, E.; Youngblood, J. P.; Moon, R. J.; Kippelen, B. *Org. Electron.* **2014**, *15*, 661.
11. Zhu, H.; Fang, Z.; Preston, C.; Li, Y.; Hu, L. *Energy Environ. Sci.* **2014**, *7*, 269.
12. Klemm, D.; Kramer, F.; Moritz, S.; Lindström, T.; Ankerfors, M.; Gray, D.; ; Dorris, A. *Angew. Chem. Int. Ed.* **2011**, *50*, 5438.
13. Zhou, Y.; Fuentes-Hernandez, C.; Khan, T. M.; Liu, J. C.; Hsu, J.; Shim, J. W.; Dindar, A.; Youngblood, J. P.; Moon, R. J.; Kippelen, B. *Sci. Rep.* **2013**, *3*, 1536.
14. Chinga-Carrasco, G.; Tobjörk, D.; Österbacka, R. *J. Nanopart Res.* **2012**, *14*, 1.
15. Zhu, H.; Xiao, Z.; Liu, D.; Li, Y.; Weadock, N. J.; Fang, Z.; Huang, J.; Hu, L. *Energy Environ. Sci.* **2013**, *6*, 2105.
16. Poplin, J. H.; Swatloski, R. P.; Holbrey, J. D.; Spear, S. K.; Metlen, A.; Gratzel, M.; Nazeeruddin, M. K.; Rogers, R. D. *Chem. Commun.* **2007**, *20*, 2025.
17. Janietz, S.; Katholing, E.; Lange, A.; Schindler, W. *Organic Photovoltaic XIV, Proc. of SPIE,* **2013**, *8830*, 883019.
18. Hu, L.; Zheng, G.; Yao, J.; Liu, N.; Weil, B.; Eskilsson, M.; Karabulut, E.; Ruan, Z.; Fan, S.; Bloking, J. T.; McGehee, M. D.; Wagberg, L.; Cui, Y. *Energy Environ. Sci.* **2013**, *6*, 513.
19. Lange, A.; Schindler, W.; Wegener, M.; Fostiropoulos, K.; Janietz, S. *Solar Energy Mater. Solar Cells* **2013**, *109*, 104.
20. Kim, J. B.; Kim, C. S.; Kim, Y. S.; Loo, Y. L. *Appl. Phys. Lett.* **2009**, *95*, 183301.
21. Woo, S.; Hyun Kim, W.; Kim, H.; Yi, Y.; Lyu, H. K.; Kim, Y. *Adv. Energy Mater.* **2014**, *4*, 7.